Journal of the Australian Ceramic Society (2022) 58:29–38
https://doi.org/10.1007/s41779-021-00664-4

RESEARCH

$A_{0.8}Er_{0.2}TiNbO_6$ (A = Ce, Pr, Nd, and Sm) functional ceramics

Fergy John[1] · **Sam Solomon**[2]

Received: 24 May 2021 / Revised: 30 August 2021 / Accepted: 20 September 2021 / Published online: 28 September 2021

Abstract
This work highlights the investigations on the structure, optical, and dielectric properties of Erbium-substituted Lathanide Titanium Niobate ceramics. The ceramics $A_{0.8}Er_{0.2}TiNbO_6$ (A = Ce, Pr, Nd, and Sm) having aeschynite orthorhombic symmetry were synthesized via conventional solid-state ceramic route method. The symmetry of the samples was determined using XRD and vibrational spectroscopic methods. Surface morphology of the sintered samples was investigated with the help of SEM technique. The optical properties of the samples were studied using UV–Vis absorption spectroscopy and the band gap was estimated using Tauc's plot. Photoluminescence spectra of Erbium-substituted Lathanide Titanium Niobate compounds indicated intense emission lines in the visible region. The studies of dielectric properties at room temperature in microwave and radio frequency regions confirmed the suitability of material in the dielectric resonator applications. Complex impedance spectroscopic studies examined the electrical properties of the samples at different temperatures. The developed samples can be treated as suitable functional ceramics for optical and dielectric applications due to its improved dielectric, optical, and sintering properties.

Keywords Ceramics · Conventional solid-state ceramic route · Vibrational spectroscopy · Dielectric properties · Impedance spectroscopy · Optical band gap

Introduction

Optically active ceramics with electrical properties can be developed through the substitution of atoms with identical valency and ionic radius in the compounds for various applications. The properties of the ceramic materials were tailored generally by substituting other suitable atoms [1, 2]. Sebastian et al. successfully developed a novel dielectric resonator material, $SmTiNbO_6$ ceramic, for the microwave communication systems [3]. The dielectric properties such as dielectric constant, quality factor, and dielectric loss of $RETiNbO_6$ ceramics in the microwave region prepared through solid-state ceramic route were reported by Sebastian et al. [4]. The ceramic having zero τ_f was developed by adjusting the concentration of aeshynite and euxenite samples in the substituted system $[RE_{1-x}RE'_x]$ $TiNbO_6$ [5]. Solomon et al. have investigated that the addition of Zinc oxide on $SmTiNbO_6$ and $DyTiNbO_6$ reduced the sintering temperature and enhanced its dielectric properties [6]. The dielectric properties of the Zinc oxide doped $LnTiTaO_6$ (Ln = Pr, Sm, and Dy) system were explored in detail [7]. The studies proved that the dielectric characteristics of the microwave ceramics $DyTiTaO_6$ have been improved by the substitution of Nb_2O_5 [8]. The dielectric properties in microwave and radio frequency region of Yttrium-substituted $NdTiTaO_6$ ceramics were reported by Kumar et al. [9]. Solomon et al. have reported the microwave dielectric properties of the zirconium-substituted sample, $Ln(Zr_{1/3}Ti_{2/3})$ TaO_6 (Ln = Ce, Pr, Nd, and Eu) ceramics [10]. The dielectric properties in microwave frequency region of Antimony-substituted $LnTiTaO_6$ system were also studied [11]. Joseph et al. have highlighted the spectroscopic and microwave investigations of Yttrium-substituted $NdTiNbO_6$ ceramics [12]. The thermally stable $Ce_xY_{1-x}TiTaO_6$ microwave ceramics have been successfully synthesized through solid-state ceramic route method with minimum dielectric loss [13]. Kumar et al. succeeded in improving the microwave dielectric

✉ Fergy John
fergyphd@gmail.com

[1] Department of Physics, St Gregorios College, Kottarakara 691531, India

[2] Department of Optoelectronics, University of Kerala, Thiruvananthapuram 695581, India

properties of $LnTiTaO_6$ (Ln = Ce, Pr, and Nd) by substituting the WO_3 and MoO_3 [14]. The systematic spectroscopic studies of $Nd_xY_{1-x}TiNbO_6$ microwave ceramics were investigated [15]. Solomon et al. have reported the effect of Eu^{3+} substitution on the photoluminescence and dielectric properties of certain microwave ceramics [16]. The microwave dielectric properties of $LnTiNbO_6$ (Ln = Nd, Sm, and Y) ceramics prepared by conventional ceramic route method have been remarkably improved by the substitution of the tin atom [17]. The microwave dielectric and optical properties of $Ln_{2/3}$ $Gd_{1/3}TiNbO_6$ (Ln = Ce, Pr, Nd, and Sm) ceramics were highlighted by A John et al. [18]. Impedance spectroscopic studies of the ceramic composite $40PrTiTaO_6 + 60YTiNbO_6$ were investigated in detail [19]. Remya et al. studied the enhanced dielectric and optical properties of $PrYTiTaO_6$ ceramic by the doping of ZnO and EuO [20]. Wang et al. reported the influence of Praseodymium atom on the dielectric properties of Stronium Titanate ceramic [21]. The nanocrystalline (Ce/Pr/Nd/Sm)$TiNbO_6$ with enhanced dielectric properties were developed by John et al. [22]. At radio frequency range, the dielectric properties such as conductance, tangent loss, and permittivity of nanocrystalline (Dy/Er/Gd/Yb)$TiNbO_6$ prepared by combustion method were investigated [23]. The substitution of Bi for Gd in $Gd_3Fe_5O_{12}$ compound reduced the sintering temperature and improved the dielectric properties [24]. The dielectric and optical properties of Lutetium-substituted Lathanide Titanium Niobate prepared by conventional solid-state ceramic methods were reported [25]. The electrical properties of pure and zirconium-substituted nanocrystalline samarium titanate were also studied [26]. In the present investigation, we are reporting the structure, dielectric, electrical, and optical behavior of Erbium-substituted Lanthanide Titanium Niobate, $A_{0.8}Er_{0.2}TiNbO_6$ (A = Ce, Pr, Nd, and Sm), ceramics synthesized through solid-state ceramic method.

Experimental

The samples $Ce_{0.8}Er_{0.2}TiNbO_6$, $Pr_{0.8}Er_{0.2}TiNbO_6$, $Nd_{0.8}Er_{0.2}TiNbO_6$, and $Sm_{0.8}Er_{0.2}TiNbO_6$ (abbreviated as CETN, PETN, NETN, and SETN) were developed using the conventional solid-state ceramic route using the stoichiometric amounts of high purity oxides and carbonates of constituent elements. The mixtures calcined at 1100 °C for 4 h were ground well using acetone as the mixing medium. The powder mixed with the binder was compressed using pelletizer to obtain the compact form of pellets. The highly dense form of the pellets was prepared through the sintering process.

Characterizations

The X-ray diffraction study was used to determine the structure of the samples (Philips Expert Pro). The phase purity and the structure of the samples were further checked by FT Raman spectrum (Bruker RFS/100S spectrometer) and FTIR spectroscopic techniques (Thermo-Nicolet Avatar 370 FT-IR Spectrometer). Thermally etched polished sample was used for studying the surface morphology with Scanning Electron Microscopy (SEM) (JEOL JSM 5610 LV). In order to calculate the dielectric parameters of the sintered samples, LCR meter (Hioki-3532–50) was used within the radio frequency range. The dielectric properties of the sintered samples were measured in the microwave frequency range using the network analyzer (Agilent 8753 ET). The optical absorption (Jasco-D550 UV–Vis spectrometer) and photoluminescence spectra (Flurolog®-3 Spectroflurometer) of the samples were recorded. Impedance analyzer was employed to investigate the electrical properties of the samples using a Hioki LCR Hi Tester, as a function of temperature and radio frequencies.

Results and discussion

Figure 1 shows the XRD patterns of the powdered samples CETN, PETN, NETN, and SETN. All the Bragg's diffraction peaks are identified by the aeschynite orthorhombic structures of $ATiNbO_6$ (A = Ce, Pr, Nd, and Sm) (ICDD file 15–0864, 20–1361, 52–1130) and $ErTiNbO_6$ (ICDD file 20–1216) with space group pnma [3, 22]. The diffraction peaks of $ErTiNbO_6$ are also indexed in the XRD pattern of

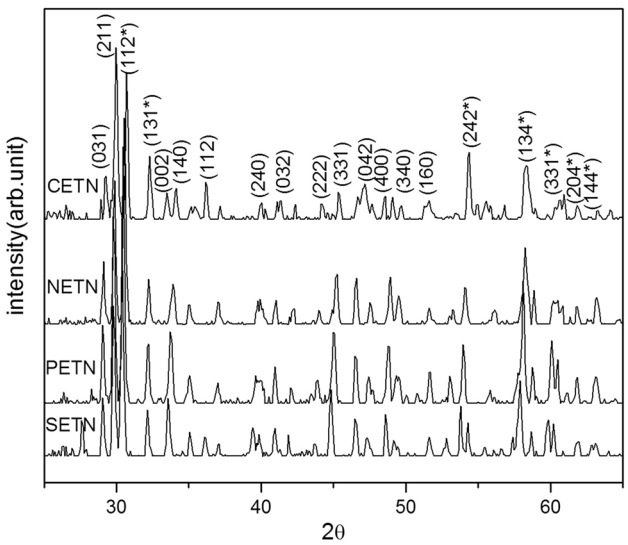

Fig. 1 XRD patterns of all the samples

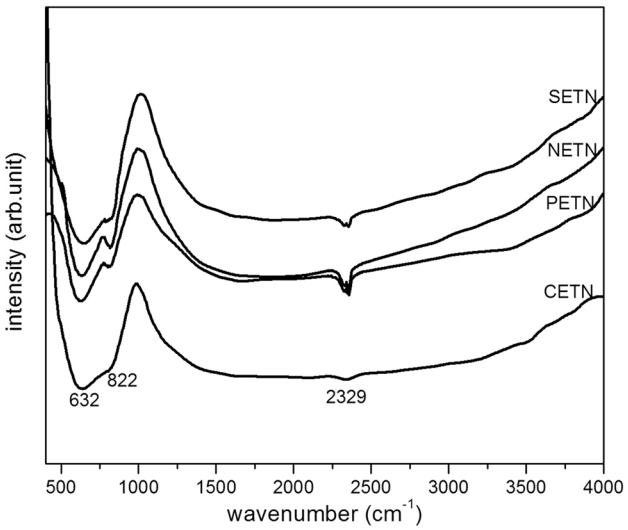

Fig. 2 FTIR spectra of all the samples

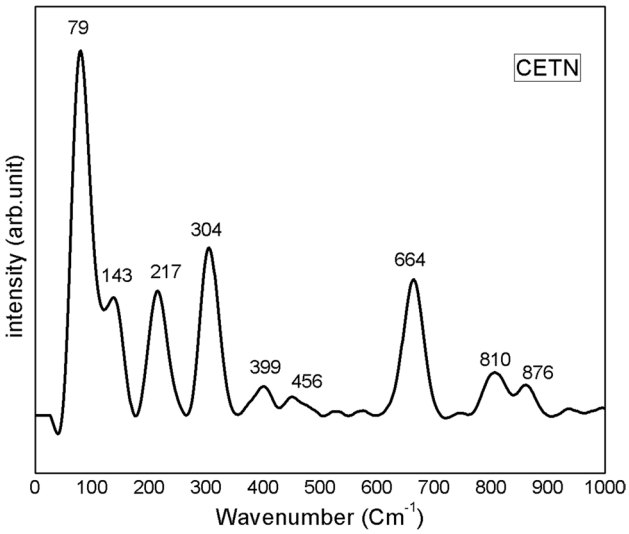

Fig. 3 Raman spectrum of CETN

the sample followed by * and substantiate the substitution of Er for the Lathanides atoms, Ce, Pr, Nd, and Sm. Erbium has comparable ionic radii with the Lathanides atoms so that it can be substituted easily.

The FT-IR spectra of the powdered samples presented in Fig. 2 established the crystallization of the structure. The bands in FT-IR spectra are assigned according to the vibrations of NbO_6 octahedra. The stretching modes of the octahedra $NbO_{6\ in}$ the sample are observed at 632 cm^{-1} with a shoulder band at 822 cm^{-1}. A prominent band at 2329 cm^{-1} is due to stretching or bending vibrations of the hydroxyl group [22]. The FTIR studies support the XRD result and prove the absence of impurity in the samples.

XRD analysis identified the substitution of Erbium into the A site of $ATiNbO_6$ (A = Ce, Pr, Nd, and Sm) with the stoichiometric formula $A_{0.8}Er_{0.2}TiNbO_6$. To confirm the structure, the FT-Raman spectrum of CETN was recorded and shown in Fig. 3. The Raman active symmetric stretching mode υ_1A_{1g} and the asymmetric stretching mode υ_2E_g of the bonds Nb–O or Ti–O are observed in the spectrum. The υ_1A_{1g} with shoulder peak at 810 cm^{-1} and υ_2E_g mode of NbO_6 or TiO_6 octahedra in the sample is appeared at 876 cm^{-1} and 664 cm^{-1}, respectively. The intensity and position of the symmetric and asymmetric stretching bands are the characteristics of orthorhombic structure. The υ_3F_{1u} mode with minimum intensity is occurred at 456 cm^{-1} in the Raman spectra of the compound. A very weak band is observed at 399 cm^{-1} in the υ_4F_{1u} region and the Raman active symmetric bending υ_5F_{2g} mode is also appeared at the wavenumber 304 cm^{-1}. The silent υ_6F_{2u} mode is also active at 217 cm^{-1} and all the lattice vibrations have appeared below 200 cm^{-1} in the Raman spectrum [27]. The vibrational modes already reported for the orthorhombic aeschynite symmetry exactly agree well with all vibrational Raman active modes of CETN. The XRD, FT IR, and FT Raman spectroscopic studies confirmed the orthorhombic symmetry and crystalline nature of the samples.

The dielectric and impedance spectroscopic measurements required maximum dense form of the sample with specific shape and size without any pores, crack, and air column. All samples sintered at 1200 °C for 4 h obtained 95% of the theoretical density within the orthorhombic structure. The partial replacement of rare earth elements with Erbium in $ATiNbO_6$ system decreased the temperature of sintering process noticeably and enhanced the densification process. The decrease in the sintering temperature of the Erbium-substituted samples was about 180 °C when compared with the pure samples [3, 4].

The grains shape and distribution of the sintered CETN and PETN samples are shown in Fig. 4a–b. The highly compact form of the samples pellets was densified without any cracks and cavities on the surface. The SEM studies revealed that the inhomogeneous grains are uniformly distributed possibly due to the presence of $ATiNbO_6$ (A = Ce, Pr, Nd, and Sm) and $ErTiNbO_6$ structures. The elongated morphology of grains was reported for orthorhombic structured rare earth titanium tantalates [28]. Here, the SEM studies also validate the results of XRD and vibrational spectroscopic studies.

The EDS spectra of the samples CETN and PETN are shown in Fig. 5a–b. Peaks due to the presence of all the constituent elements such as Cerium, Praseodymium, Erbium, Titanium, Niobium, and oxygen in the samples are appeared at the different values of the binding energy. The mass percentage and atomic percentage of the constituents elements present in the samples are also shown in EDS spectra. The

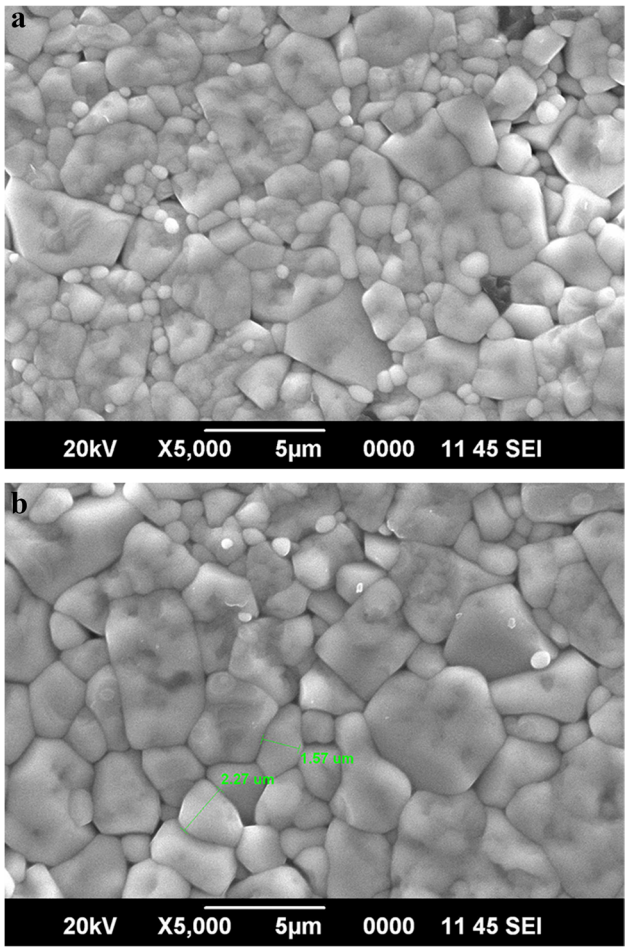

Fig. 4 SEM micrographs of the samples **a** CETN and **b** PETN

EDS analysis confirms that all the constituent elements are present in sample according to the expected stoichiometric concentrations.

Dielectric permittivity and quality factor in the Microwave frequencies of all the samples were investigated. The dielectric constant in this frequency is estimated as 40, 36, 35, and 32 for CETN, PETN, NETN, and SETN, respectively at room temperature. Similarly, the quality factor ($Q_u \times f$) for CETN, PETN, NETN, and SETN is found to be 11,870, 17,860, 14,590, and 14,370, respectively at the microwave frequency range. When compared to the microwave properties of the pure samples reported by Sebastian et al., Erbium in $ATiNbO_6$ (A = Ce, Pr, Nd, and Sm) ceramics increases the quality factor along with the high dielectric constant [4]. The Erbium-substituted ceramics can improve the selectivity and sharpness of the signal in the microwave communication system.

For the sintered samples, typical differences can be seen for the dielectric permittivity (ε_r), tangent loss (tan δ), and conductance (G), with radio frequencies. As shown in Fig. 6, only at upper-frequency side dielectric constant reaches a stable value due to interfacial polarization reported by Maxwell and Wagner [29]. The reduction in the value of dielectric permittivity or dielectric constant at low frequency range is due to the delay in polarization of charges which possess inertia when electric field is applied. The value of dielectric permittivity at 1 MHz is estimated to be 36 for SETN, 43 for NETN, and 45 for both PETN and CETN samples.

At low radio frequency side, the value of ac conductance of the ceramics is constant up to 1 MHz as shown in Fig. 7. But it increases with the increasing in frequency as explained by Koop's phenomenological model. The sample shows the lowest value of dielectric loss (tan δ) at high frequency range as shown in Fig. 8 [30]. The decrease in tangent loss and dielectric permittivity at higher frequency side is due to the mobile charge carriers in the dielectric ceramics. The electrical energy dissipation at radio frequency range is very low for all the samples. It is interesting to note that these parameters became almost frequency independent at higher frequency region. The dielectric studies gave the evidence that these samples can be used as the dielectric of the resonator capacitors in the communication circuits.

The prepared nanopowder sample (0.01 g) was dispersed in 10 ml ethanol. Absorption spectra of the resultant transparent solution in the ultraviolet and visible regions were taken. Figure 9a–d gives the optical absorption spectra of the samples plotted in the wavelength ranges from 300 to 700 nm. Several investigators have reported that the bands corresponding to the absorption of wavelength in the visible region produced by trivalent lanthanide ions most probably originate in the 4f energy level [31]. From the UV absorbance studies, it was observed that the samples absorbed the entire wavelength of the ultraviolet region only but feasible absorption in the visible wavelength region. The electrons in the higher principal quantum number orbitals of the atoms in the samples screened the inner orbitals from external influences. As a consequence, the UV–Vis spectrum consists of distinct and characteristic bands. The bands due to absorption of wavelength at 550–600 nm in the spectra of the as-prepared samples are broadened due to the strong influence of chemical environmental factors like Ti^{4+} and Nb^{5+} ions. The different peaks at 440–540 nm can be seen in all the obtained spectra due to the transition of Er^{3+} ions [32]. The absorption spectra showed bands around 420–490 nm due to the transitions that confirmed the occupancy of Ce^{3+}, Pr^{3+}, Nd^{3+}, and Sm^{3+} ions in a single site [33, 34]. The characteristic transition bands of Niobium ions can be seen in the wavelength range 580–620 nm. The peaks in the range of 290–350 nm were due to the presence of defect levels of Erbium ions. The optical absorption studies depicted that the developed samples are good candidates for UV filter and sensor applications.

The UV–Vis absorption coefficient of the material which depends on photo energy was stated by Tauc's

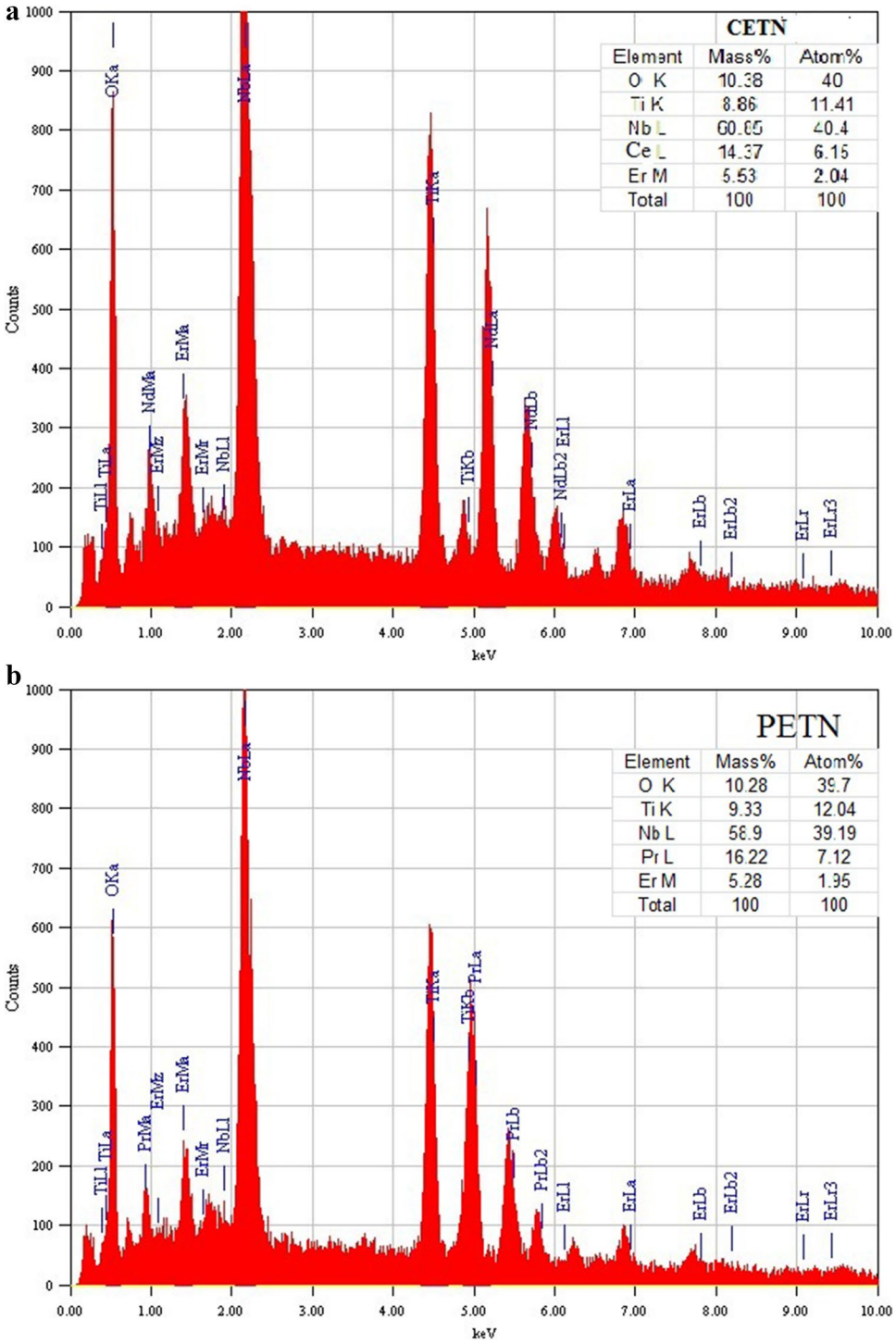

Fig. 5 EDS spectra of the samples **a** CETN and **b** PETN

equation, $(\alpha h\upsilon) = B(h\upsilon - E_g)^m$, where α is the absorbance, h is Planck's constant, ν is the frequency, B is the energy-independent constant, E_g is the optical energy gap, and m is the constant associated to the different types of electronic transitions ($m = 1/2$ for direct allowed, $m = 2$ for indirect allowed, $m = 3/2$ for direct forbidden, and $m = 3$ for indirect forbidden transitions). The allowed electronic transitions dominate the basic absorption processes giving direct or indirect transitions. Among all possible transitions, $m = 1/2$ gives the best fit linearly in the band-edge region of Tauc's plot for all the samples, and hence, the samples showed the direct allowed electronic transitions. The direct allowed optical band gap can be obtained from the intercept of the linear region with the axis $(\alpha h\nu)^2 = 0$ [35]. Tauc's plots of all the samples are shown in Fig. 10a–d.

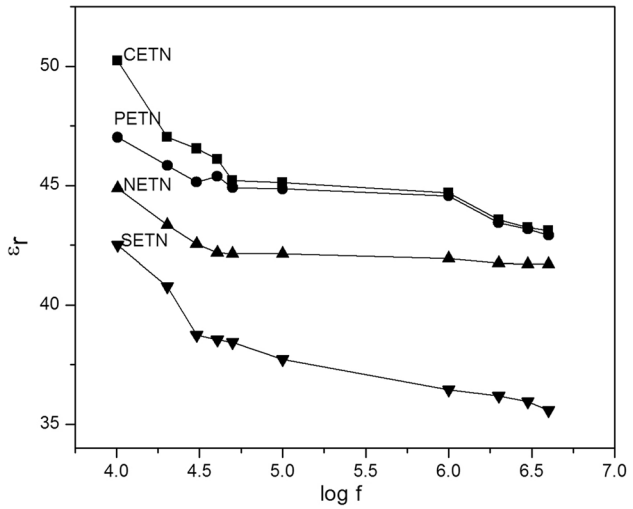

Fig. 6 Variation of dielectric constant with frequency of all samples

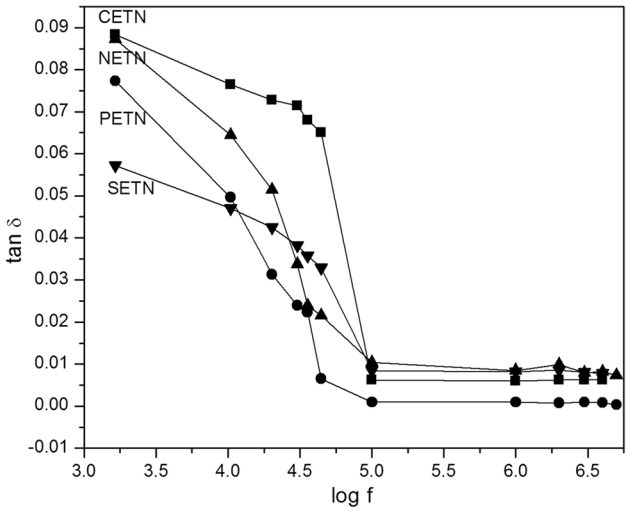

Fig. 8 Variation of loss factor with frequency of all samples

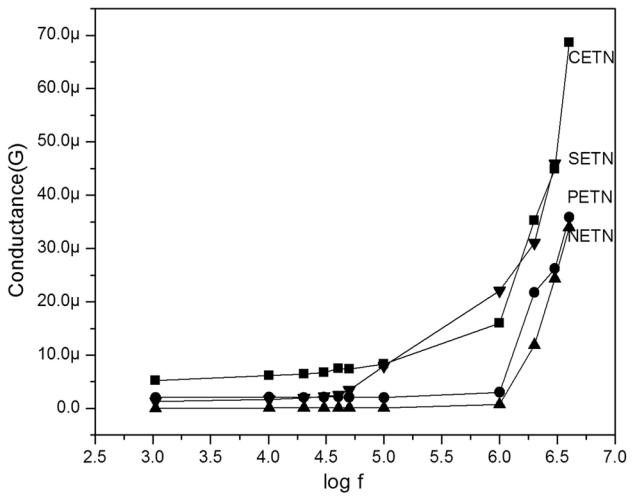

Fig. 7 Variation of conductance with frequency of all samples

The optical band gap of CETN, PETN, NETN, and SETN is estimated to be 3.24, 2.96, 2.9, and 3.1 eV, respectively.

The photoluminescence spectra obtained at the excitation wavelength 270 nm of the sample presented in Fig. 11a–b exhibit strong emissions in the visible range of wavelength. The peaks corresponding to the transitions of the constituent elements in the samples were recognized on the basis of Payling and Larkins data [36]. The emission lines observed at 370 nm, 423 nm, 448 nm, 494 nm, 538 nm, and 600 nm are due to $^{3}F_{4}$–$^{0}A^{\circ}_{3}$ of Er atom, $^{4}D_{2.5}$–$^{2}D^{\circ}_{2.5}$ of Nb atom, (12.5, 2.5)°10–$^{0}A_{9}$ of Er atom, $^{7}F_{3}$–$^{5}F^{\circ}_{3}$ of Sm atom, $^{6}L_{5.5}$–$^{0}A^{\circ}_{6.5}$ of Pr atom, and $^{5}F_{3}$–$^{3}F^{\circ}_{3}$ transition of Ti atom. The photoluminescence property evidences that the samples can be suitable for several optoelectronic systems.

Materials having good ionic conductivity are the essential components of solid oxide fuel cells and other energy sources. The thermally triggered O^{2-} ions hopping inside the lattice space of the sample establish conduction in the ceramics [37]. The impedance studies of the sample NETN were conducted at different temperatures. Figure 12a–b shows the behavior of Z′ (real part of impedance) with radio frequencies at 100–700 °C. The value of Z′ falls against both the frequency and temperature pointed out the ac conductivity of the ceramic samples and its negative temperature coefficient of resistance behavior. But the values of Z′ coincide in higher frequency region due to the discharge of space charges and the conductivity of the sample increases with temperature.

Figure 13a–b which presents the plot of Z″ (imaginary part of impedance) with frequency indicates that the value of Z″ has decreased and the peak maxima shifted to high frequency region at high temperatures. Widening of the peaks is due to the spreading of relaxation time in the sample. The electrical behavior of the ceramic samples at various temperatures was studied using the impedance plot shown in Fig. 14a–b. At low-temperature plot is a straight line with large slopes that indicates the non-conducting nature of the ceramic material. But the slopes of the lines decrease and bend towards the Z′-axis with increasing temperature and two semicircles are formed. The semicircles are obtained due to the contributions of grains and its boundary in the conductivity of the ceramic samples. The nature of impedance spectrum showed the evidence of the negative temperature coefficient of resistance behavior of the sample identical to a semiconductor. This semiconducting nature of ceramic might be due to the presence of oxygen deficiency during high-temperature sintering process [38–40]. Impedance studies revealed that the sample can be used as electrolyte

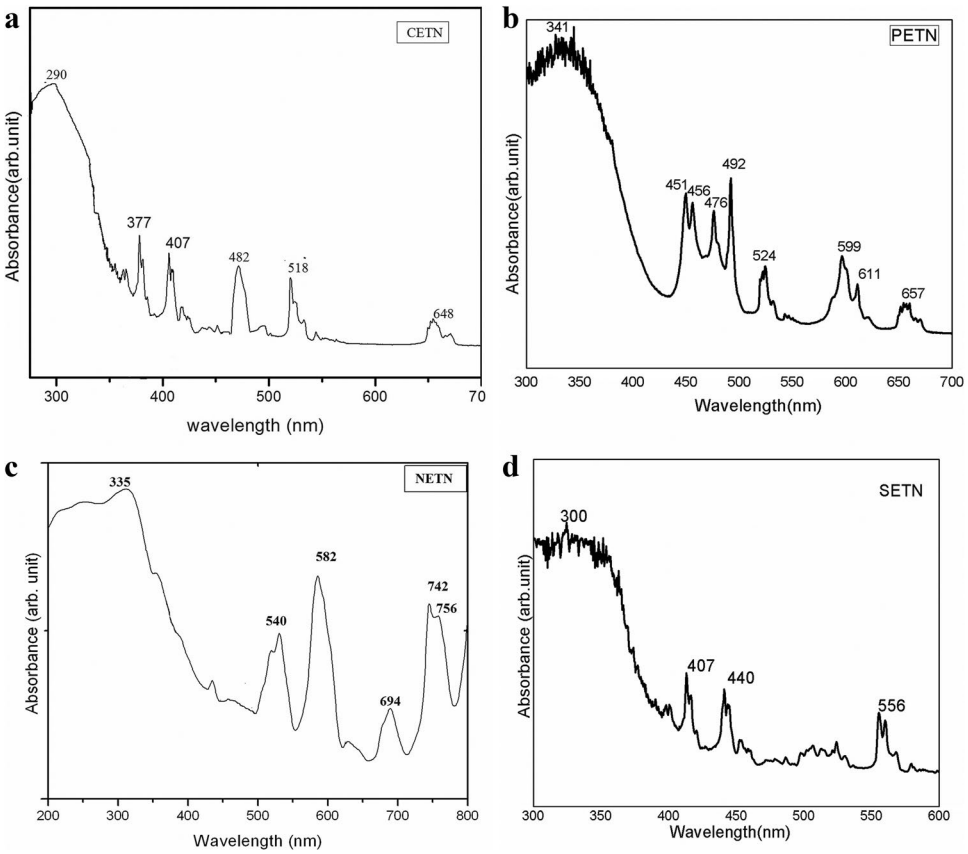

Fig. 9 **a–d** UV–Vis absorption spectra of all the samples

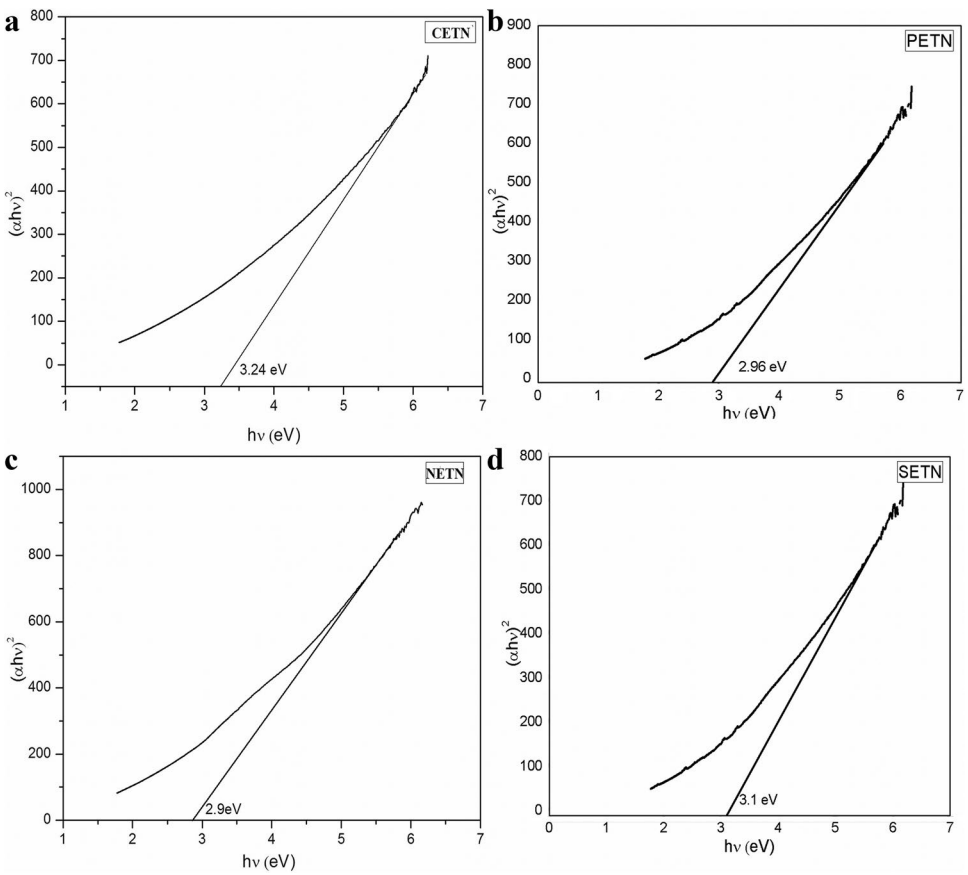

Fig. 10 **a–d** Tauc's plots of all the samples

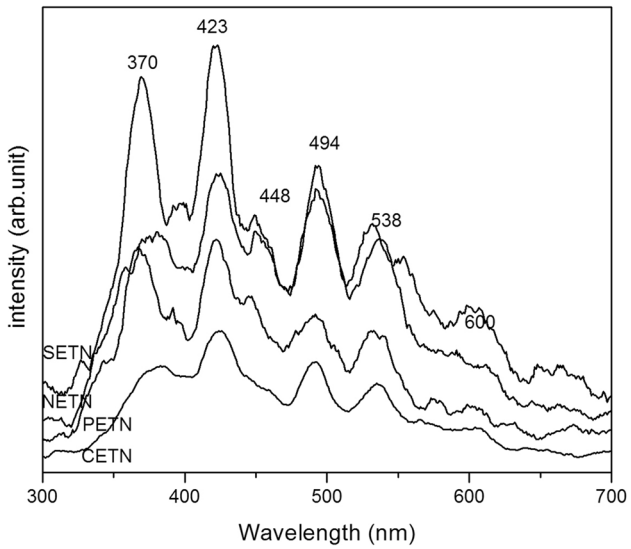

Fig. 11 PL emission spectra of the samples

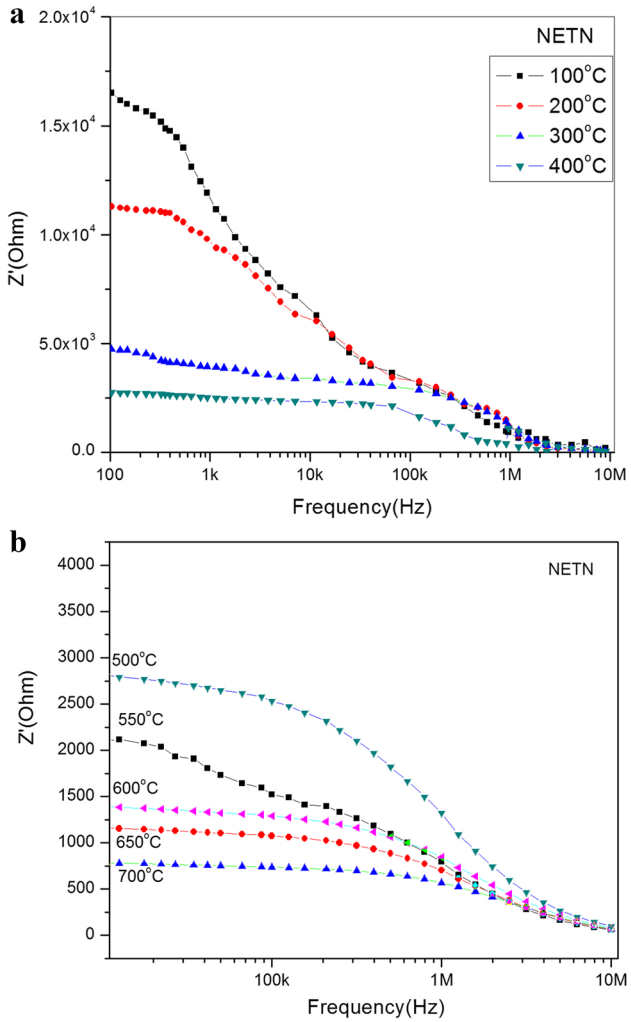

Fig. 12 **a–b** Real part of impedance with frequencies of NETN at 100–700 °C

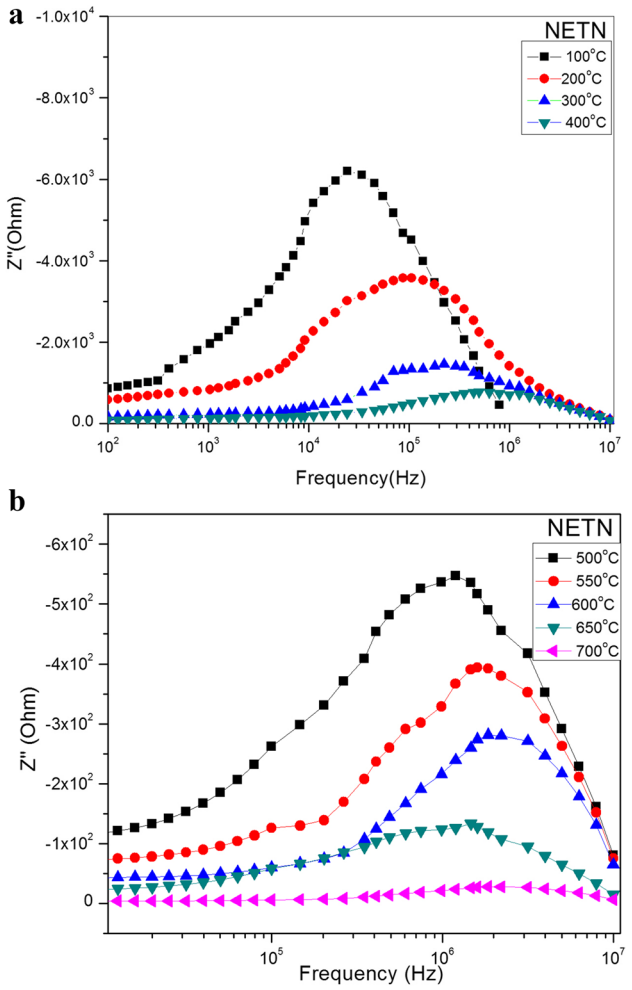

Fig. 13 **a–b** Imaginary part of impedance with frequencies of NETN at 100–700 °C

in solid oxide fuel cells due to the optimum ionic conductivity of the samples at high temperatures.

Conclusions

The solid-state ceramic route was used to produce the samples $Ce_{0.8}Er_{0.2}TiNbO_6$, $Pr_{0.8}Er_{0.2}TiNbO_6$, $Nd_{0.8}Er_{0.2}TiNbO_6$, and $Sm_{0.8}Er_{0.2}TiNbO_6$. X-ray structural study revealed the orthorhombic aeschynite symmetry of the samples and the vibrational spectroscopic studies confirmed the XRD results. The surface morphology of the samples showed the inhomogeneous distribution of grains of both $ATiNbO_6$ (A = Ce, Pr, Nd, and Sm) and $ErTiNbO_6$ all over the sample. The UV–Vis spectra analysis revealed that the samples are wide band gap material showing good absorbance in the ultraviolet region. The optical band gap of CETN, PETN, NETN, and SETN using Tauc's plot are investigated to be 3.24, 2.96, 2.9, and 3.1 eV, respectively. The high Q-factor and high dielectric

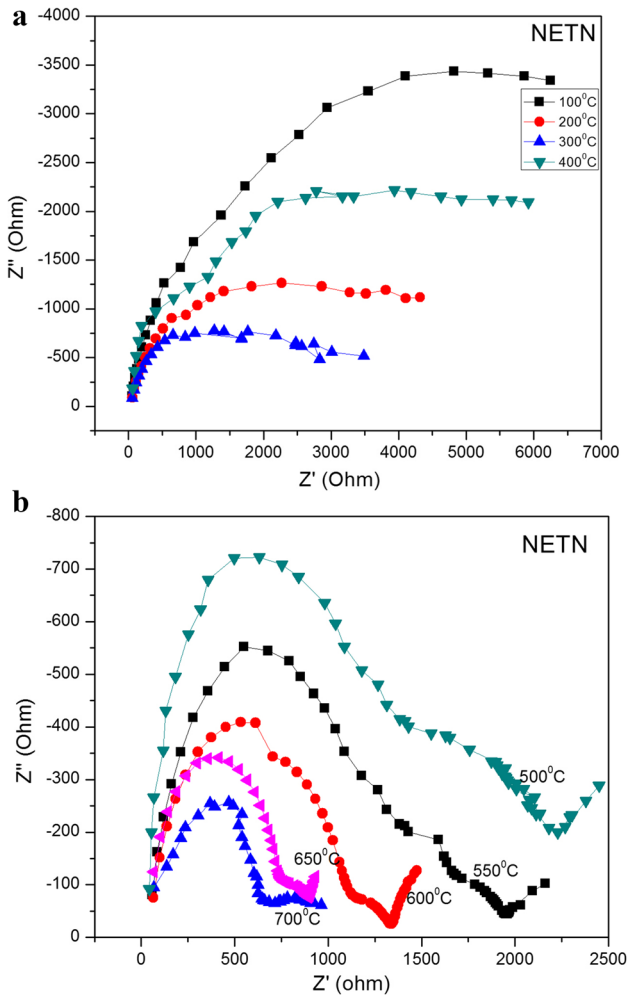

Fig. 14 **a–b** Complex impedance spectra of NETN at 100–700 °C

permittivity of samples in both radio and microwave frequency region make the samples potential candidates for dielectric resonator applications in communication systems. The samples are also found to be a luminescent material with some emission peaks at the visible region. The grain and grain boundary contribution to the ionic conductivity of the ceramics at different temperatures are established through impedance spectroscopic studies. The decrease in sintering temperature, excellent dielectric and photoluminescence properties, and enhanced ionic conduction at high temperatures are due to the substitution of Erbium in $ATiNbO_6$ (A = Ce, Pr, Nd, and Sm) ceramics. These conventionally prepared samples are investigated as a functional ceramics for optical, dielectric, and solid oxide fuel cell applications.

Author contribution The authors are responsible for all the descriptions and writing—original draft preparation and results.

Availability of data and material Not applicable.

Code availability Not applicable.

Declarations

Ethics approval Not applicable.

Consent to participate Not applicable.

Consent for publication Not applicable.

Competing interests The authors declare no competing interests.

References

1. Guoqing, W., Shunhua, W., Hao, S.: Microwave dielectric ceramics in the BaO–TiO_2 ZnO system doped with $MnCO_3$ and SnO_2. Mater. Lett. 59, 2229 (2005)
2. Zou, J.-L., Zhang, Q.-L., Yang, H., Sun, H.-P.: A new system of low temperature sintering ZnO–SiO_2 dielectric ceramics. Jpn. J. Appl. Phys. **45**, 4143–4145 (2006)
3. Sebastian, M.T., Ratheesh, R., Sreemoolanathan, H., Solomon, S., Mohanan, P.: Samarium titanium niobate ($SmTiNbO_6$) – a new microwave dielectric ceramic. Mater. Res. Bull. **32**(9), 1279 (1997)
4. Sebastian, M.T., Solomon, S., Ratheesh, R., George, J., Mohanan, P.: Preparation, characterization and microwave properties of $RETiNbO_6$ (RE = Ce, Pr, Nd, Sm, Eu, Gd, Tb, Dy, Y and Yb) dielectric ceramics. J. Am. Ceram. Soc. **84**, 1487–89 (2001)
5. Solomon, S., Kumar, M., Surendran, K.P. , Mohanan, P., Sebastian, M.T.: Synthesis, characterization and properties of $[RE_{1-x}RE'_x]TiNbO_6$ dielectric ceramics. Mater. Chemi. Phys. **67**, 291–293 (2001)
6. Solomon, S., Joseph, J.T., Padma Kumar, H., Thomas, J.K.: Effect of ZnO doping on the microwave dielectric properties of $LnTiNbO_6$(Ln=Sm or Dy) ceramics. Mater. Lett. **60**, 2814–2818 (2006)
7. Padma Kumar, H., Joseph, J.T., Thomas, J.K., RaamaVarma, M., John, A., Solomon, S.: Influence of zinc oxide addition on $LnTiTaO_6$ (Ln = Pr, Sm and Dy) materials for dielectric resonators. Mater. Sci. Eng. B. **143**, 51–54 (2007)
8. Joseph, J.T., Kumar, H.P., Varma, M.R., Thomas, J.K., Solomon, S.: Effect of Nb_2O_5 substitution on the dielectric characteristics of $DyTiTaO_6$ microwave ceramics. Mater. Lett. **62**, 1064–1066 (2008)
9. Kumar, H.P., Thomas, J.K., Varma, M.R., Solomon, S.: Synthesis and characterization of thermally stable, high Q, $Nd_xY_{1-x}TiTaO_6$ dielectric resonators. J. Alloys. Compd. **455**, 475 (2008)
10. Solomon, S., Kumar, H.P., Jacob, L., Thomas, J.K., Varma, M.R.: Ln $(Zr_{1/3}Ti_{2/3})TaO_6$ (Ln= Ce, Pr, Nd and Eu): A novel group of microwave ceramics. J. alloy. compd. **461**(1–2), 675–677 (2008)
11. Kumar, Joseph, S., Solomon, S., Varma, M.R., Thomas, J.K.: Synthesis, structure analysis, and microwave dielectric properties of $LnTiSb_xTa_{1-x}O_6$ (Ln=Ce, Pr, and Nd) ceramics. Int. J. Appl. Ceram. Technol. **5**(4), 347–352 (2008)
12. Joseph, J.T., Padma Kumar, H., Varma, M.R., Thomas, J.K., Solomon, S.: Synthesis and characterization of thermally stable, high Q, $Nd_xY_{1-}xTiTaO_6$ dielectric resonators. Mater. Lett. **62**, 1064 (2008)
13. Padma Kumar, H., Vijayakumar, C., Thomas, J.K., Raamar Varma, M., Solomon, S.: Synthesis of low loss, thermally stable

$Ce_xY_{1-x}TiTaO_6$ microwave ceramics. Mater. Resea. Bull. **44**, 276–279 (2009)
14. Kumar, H.P., Suresh, M.K., Thomas, J.K., John, A., George, B., Solomon, S.: Effect of WO_3 and MoO_3 addition on $LnTiTaO_6$ (Ln= Ce, Pr and Nd) microwave ceramics. J. Alloys Compd **478**(1–2), 648–652 (2009)
15. Joseph, S., Suresh, M.K., Thomas, J.K., John, A., Solomon, S.: Synthesis, characterization, and spectroscopic analysis of $Nd_xY_{1-x}TiNbO_6$ microwave ceramics. Int. J. Appl. Ceram. Technol. **7**, E129 (2009)
16. Solomon, S., Jacob, L., Kumar, H.P., Gopchandran, K.G., Thomas, J.K.: Photoluminescence and dielectric properties of Eu^{3+} substituted microwave ceramics. J. Mater. Sci. Mater. Electron. **21**(11), 1132–1136 (2010)
17. Solomon, S.: Synthesis and characterization of Sn substituted $LnTiNbO_6$ (Ln=Nd, Sm and Y) microwave ceramics. I. J. appli. ceram. techn. **71**, 315–321 (2010)
18. John, A., Joseph, S., Manu, K.M., Thomas, J.K., Solomon, S.: Structure, microwave dielectric and optical properties of $Ln_{2/3}Gd_{1/3}TiNbO_6$ (Ln= Ce, Pr, Nd and Sm) ceramics. J. Mater. Sci. Mater. Electron. **22**(7), 776–780 (2011)
19. Dhwajam, D.B., Suresh, M.B., Hareesh, U.S., Thomas, J.K., Solomon, S., John, A.: Impedance and modulus spectroscopic studies on $40PrTiTaO_6$+ $60YTiNbO_6$ ceramic composite. J. Mater. Sci. Mater. Electron. **23**(3), 653–658 (2012)
20. Remya, G., Dhwajam, D., Thomas, J., Solomon, S., John, A.: Dielectric and optical properties of ZnO and EuO doped $PrYTiTaO_6$ ceramic. J. Mater. Sci.: Mater. Electron. **23**(2), 370–375 (2012)
21. Xia of ei Wang, Qi ubo Hu, Li, L., Lu X.: Effect of Pr substitution on structural and dielectric properties of $SrTiO_3$. J. Appl. Phys. **112**, 044106 (2012)
22. John, F., John, A., Thomas, J.K., Solomon, S.: Electrical and optical properties of nanocrystalline RE–Ti–Nb–O_6 (RE = Ce, Pr, Nd and Sm) electronic material. J. Mater. Sci: Mater Electr. **28**, 5997–6007 (2017)
23. John, F., Jacob, J., Thomas, J.K., Solomon, S.: Electrical and optical properties of nano-crystalline RE-Ti-Nb-O_6 (RE = Dy, Er, Gd, Yb) synthesized through a modified combustion method. J. Asian Ceram. Soc. **5**(2), 151–159 (2017)
24. Rajan, A., Das, S., Sibi, K.S. , Subodh, G.: Influence of Bi substitution on the microstructure and dielectric properties of $Gd_3Fe_5O_{12}$ ceramics. J. Electr. Mater. **48**, 1133–1138 (2019)
25. John, F., Solomon, S.: Dielectric and optical properties of $Ln_{0.8}Lu_{0.2}TiNbO_6$ (Ln= Ce, Pr, Nd & Sm) ceramics. Phys. Lett. A **384**(28), 126731 (2020)
26. Sandeep, K., Thomas, J.K., Solomon, S.: Structure and properties of pure and zirconium substituted nanocrystalline samarium titanate. Mater. Sci. Eng. B **254**, 114512 (2020)
27. Nakamoto, K.: Infrared and Raman spectra of inorganic and coordination compounds, 4th edn. Wiley, New York (1986)
28. Oishi, T., Kan, A., Ohsato, H., Ogawa, H.: Crystal structure microwave dielectric property relations in $Sm(Nb_{1-x}Ta_x)$ $(Ti_{1-y}Zr_y)O_6$ ceramics. J. Euro. Ceram. Soci. **26**, 2075–2079 (2006)
29. J.C. Maxwell: A treatise on electricity and magnetism. Oxford University Press, Oxford, **2**, 328(1954)
30. Koops, C.G.: On the dispersion of resistivity and dielectric constant of some semiconductors at audio frequencies. Phys. Rev. **83**, 121 (1951)
31. Charles, M.W., Nick, H., Jr., Gregory, E.S.: Physical properties of semiconductors, 49th edn. Prentice-Hall, Englewood Cliffs (1989)
32. Skoog D.A., F. James Holler and T.A. Nieman: Principles of instrumental analysis. Harcourt Asia Pte Ltd, 5th edn. pp. 335– 337
33 Xiu, Z., Lou, M., Liu, S., Zhou, G., Zhang, H.: Synthesis and photoluminescence of Ce^{3+} doped barium haloapatites nano crystals. J. Alloy. Comp **416**, 236–238 (2006)
34. Qi, X., Hun, T.P.J., Gallangher, H.G., Henderson, B., Illingworth, R., Ruddock, I.S.: Optical spectroscopy of $PrTiNbO_6$, $NdTiNbO_6$ and $ErTiNbO_6$. J. Physi.: Conde. Matter. **8**, 4837–45 (1996)
35 Tauc, J.: Amorphous and liquid semiconductors, p. 159. Plenum, New York (1974)
36. Payling, R., Larkins, P.: Optical emission lines of elements, 1st edn. John Wiley and sons, New York (2000)
37. Gupta, V., Mansingh, A.: Hopping conduction in insulating RF-sputtered zinc oxide films. Phys. Rev. B **49**, 1989–1995 (1994)
38. Das, B.P., Choudhary, R.N.P., Mahapatra, P.K.: Impedance spectroscopy analysis of $(Pb_{0.93}\,Gd_{0.07})(Sn_{0.45}Ti_{0.55})_{0.9825}\,O_3$ ferroelectrics. Indian J. Engine. Mater. Sci. **15**, 152–156 (2008)
39. Fei Liu, S., Jun Wu, Y., Li, J., Ming Chen, X.: Effects of oxygen vacancies on dielectric, electrical, and ferroelectric properties of $Ba_4Nd_2Fe_2Nb_8O_{30}$ ceramics. Appl. Phys. Lett. **104**, 082912 (2014)
40. Ciomaga, Cristina E., Buscaglia, Maria T., Buscaglia, Vincenzo, Mitoseriu, Liliana: Oxygen deficiency and grain boundary-related giant relaxation in Ba(Zr, Ti)O3 ceramics. J. Appl. Phys. **110**, 114110 (2011)